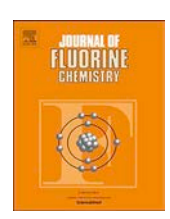
ELSEVIER

Contents lists available at ScienceDirect

Journal of Fluorine Chemistry

journal homepage: www.elsevier.com/locate/fluor



Perfluoroalkylated anthracene endoperoxide: Synthesis, characterization, crystal structure analysis, and computational insights



Anjaneyulu Putta, Andrew G. Sykes, Haoran Sun*

Department of Chemistry and Center for Fluorinated Functional Materials, University of South Dakota, Vermillion, SD, 57069, United States

ARTICLE INFO

Keywords: Endoperoxide Anthracene Fluorine Perfluoroalkylation X-ray crystallography Crystal structure

ABSTRACT

Aromatic endoperoxides serve as important intermediate species toward generating singlet state oxygen, which is key to photodynamic therapy applications. Gaining insights for fine-tuning endoperoxide stability and degree of oxygen-oxygen bond activation is of fundamental and practical interest for the chemical and medicinal communities. We report here that 9,10-bisperfluorooctyl-anthracene, upon exposing to light and air, is almost quantitatively converted to 9,10-bisperfluorooctyl-anthracene endoperoxide (compound 1) at room temperature. ¹H NMR spectra and the X-ray crystal structure revealed that the resulting compound 1 is stable at room temperature without further decomposition. The crystal structure analysis showed that the compound 1 is stabilized by F-O intramolecular interactions along with F-F, F-H and F-C intermolecular interactions. DFT calculations further indicate that the degree of oxygen-oxygen bond activation in anthracene endoperoxides, reflected as changes of O-O, C-O bond distances, may not solely depend on the electronic effect of substituents at the 9,10- positions. This uncertainty warrants further investigation both experimentally and computationally.

1. Introduction

Aromatic endoperoxides are molecules that contain an O–O bond that bridges two carbon atoms within an arene ring. They possess important applications in material sciences [1–3] and medicine [4,5]. Of particular interest is the application of aromatic endoperoxides in photodynamic therapy, where singlet oxygen $(^{1}O_{2})$ is generated from light absorption dyes and used to destroy cancerous tumor cells [6–15]. The commonly used arenes for singlet oxygen generation include rubrene [16,17], naphthalene [18,19] and anthracene [20,21]. Among the aromatics, anthracene endoperoxides have attracted considerable attention as they form singlet oxygen $(^{1}O_{2})$ through cycloreversion to anthracene with good quantum yields [20–22].

Studies on anthracene endoperoxides and generation of singlet oxygen have mostly been confined to electron donating groups (methyl, phenyl and their derivatives) substituted at the 9,10-positions of the anthracene ring. Anthracene endoperoxides with electron donating groups at the 9,10- positions often further decompose to products such as diepoxide, 9,10-dihydroxy-9,10-dihydro anthracene, 9-hydroxy-10-anthrone and anthraquinone [23–27]. A relative stable anthracene endoperoxide derivative that can generate singlet oxygen by cyclor-eversion to corresponding anthracene derivative is needed for photocatalytic applications. Fine-tuning the chemistry of endoperoxide

generation and stability of the endoperoxide products by varying ring substituents is likely one of the key steps for design of highly stable photocatalysts for generating singlet oxygen.

Fluorine, the most electronegative element, has ubiquitous applications in pharmaceuticals [28-31], agricultural chemicals [32,33] and material sciences [34–37]. Due to the high electronegativity of fluorine, perfluorocarbons (PFCs) possess excellent oxygen affinity and have been used as blood substituents [38]. Trifluoromethyl (CF₃) group were used to improve hydrolytic and oxidative stability of Artemisinin to increase half-life of the drug used for anti-malarial treatment [39]. Due to their strong electron withdrawing ability, perfluoroalkyl groups are added to aromatic cores to improve the air-stability of the n-type organic semiconductor materials [40-43]. Jones et al., found that by adding perfluoroalkyl groups onto the N, N' positions of perylene bisimide, the LUMO energy is lowered as well as the perfluoroalkyl groups created a dense close-packed barrier that prevents oxygen intrusion. Further, due to the super hydrophobic nature, perfluoroalkyl groups limit the access of proton source to aromatic core thereby improves the air-stability of organic semiconductor materials [44]. Addition of perfluoroalkyl groups onto aromatic core is one of the effective strategy to improve intermolecular interactions and π - π stacking which in turn enhance the charge transport properties of materials [45-47]. Study by Facchetti et al., found that addition of perfluoroalkyl

E-mail address: Haoran.Sun@usd.edu (H. Sun).

^{*} Corresponding author.

groups onto thiophene ring promotes better π - π stacking and higher number of non-covalent interactions compared to the corresponding alkylated analogues [48].

Herein we describe the synthesis of 9,10-bisperfluorooctyl-anthracene endoperoxide (compound 1) and its characterization via NMR and single crystal X-ray diffraction. To the best of our knowledge, this crystal structure is the first of its kind where strong electron withdrawing groups are present at the 9,10- positions of the anthracene endoperoxide molecule. To further gain insights of how different types of intermolecular interactions play a role in crystal structure stabilization, Hirshfeld surface (HS) analysis was employed to quantitatively analyze the role of various interactions that lead to the stability in the crystal lattice [49]. Together with DFT calculations, we hope that this work will shine some light on understanding how perfluoroalkyl substituents affect the physico-chemical properties of the substrates through both traditional electronic effects and non-covalent inter- and intramolecular interactions.

2. Results and discussion

2.1. NMR studies

Formation of 9,10-bisperflurooctyl-anthracene endoperoxide (compound 1) was monitored periodically by ^1H NMR spectra upon exposing the 9,10-bisperflurooctyl-anthracene in CDCl $_3$ solution to solar light (300 W 1.5 AM Xe light) in the presence of atmospheric oxygen. The formation of anthracene endoperoxide is clearly supported by ^1H NMR spectroscopy (Fig. 1). Followed by the light illumination, the anthracene resonance signals at 8.43 ppm (H $_a$) and 7.62 ppm (H $_b$) disappear, the resulting anthracene endoperoxide (compound 1) signals appear at 7.58 ppm (H $_a$) and 7.34 ppm (H $_b$). Fig. 1 indicates that 9,10-bisperflurooctyl-anthracene undergoes photooxidation to yield the compound 1 in less than 5 min. ^1H NMR results indicate that the electron delocalization across the central ring of anthracene is lost due to the formation of O $_2$ bridge bond between two carbon atoms at the 9,10 positions of the anthracene moiety. However, electron delocalization

adjacent to the central anthracene ring on either side was present. 9,10-Bisperflurooctyl-anthracene undergoes rapid and quantitative [4 + 2] cycloaddition reaction with triplet state oxygen to form endoperoxide species. Continuous exposure of this endoperoxide (compound 1) sample to solar light gives no change in $^1\mathrm{H}$ NMR spectra (Fig. 1, 5 min. to 20 min.). This result indicates that compound 1 is stable in solution, at room temperature without further decomposition. A good quality single-crystal was isolated by slow evaporation of a deuterated chloroform solution after exposing the solution to solar light confirmed the formation of compound 1.

2.2. Crystal structure analysis

Compound 1 is produced by reaction of 9,10-bisperfluorooctyl-anthracene with oxygen under light irradiation. An O–O bridge forms across the two carbon atoms at the 9,10-positions of the central anthracene ring, and breaks the π -conjugation along the anthracene moiety. This leads to two isolated benzene rings on either side of the bridged central ring with a non-planar structure. The X-ray crystal structure (Fig. 2) of compound 1 confirms the formation of anthracene endoperoxide. In the central ring where the carbon atoms directly connected to the oxygen atoms, the average C–C distance was found to be 1.523 Å, representing typical C–C single bond. The C=C double bond distances on either side of the central ring were found in between 1.380–1.394 Å. Couple of deviations were observed between C11-C12 (1.400 Å) and C13-C14 (1.416 Å) respectively. The presence of peroxide bridge in the central ring induced strain in the vicinity of bonding environment that leads to deviation from the ideal C–C bond distances.

Single crystal X-ray diffraction data reveal that compound 1 crystallizes in the centrosymmetric monoclinic P21/c space group with Z = 4. One of the terminal CF₃ groups in the crystal structure of the compound 1 has disorder due to flexibility of the chain. Disorder was treated by modeling the rotation of the CF₃ group with two occupancies. The larger 75 % occupancy is left anisotropic and the smaller 25 % occupancies are treated as isotropic. The crystal packing of compound 1 shows the presence of $C_{(sp3)}$ -F···O intramolecular interactions. The shortest distance of 2.740 Å of F···O intramolecular contact is

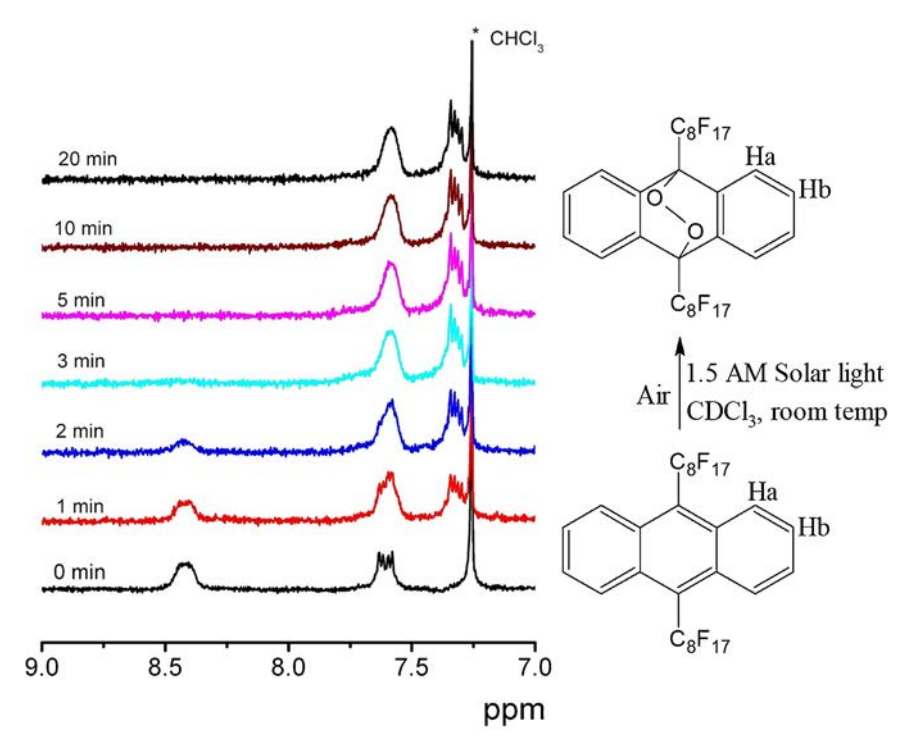


Fig. 1. Monitored ¹H NMR spectra for the conversion of 9,10-bisperfluorooctyl-anthracene (bottom structure) to corresponding endoperoxide (top structure, compound 1) in air-saturated CDCl₃ solution under 1.5 AM solar light (300 W Xe lamp) at room temperature.

Table 1O-O and C-O bond distances in anthracene endoperoxide derivatives.

Substituents	NH_2	ОН	OEt	Me(2)	Ph(3)	H(4)	C1	F	CF ₃	C_8F_{17}	C_8H_{17}	CN	NO_2
$d_{O-O}/\mathring{A}^{(a)}$ $d_{O-O}/\mathring{A}^{(b)}$	1.474	1.467	1.462	1.468 1.475	1.459 1.484	1.477 1.476	1.482	1.468	1.460	1.453 1.476*	1.464	1.466	1.472
$d_{\text{C-O}}/\text{Å}^{(a)}$ $d_{\text{C-O}}/\text{Å}^{(b)}$	1.492	1.486	1.483	1.472 1.478	1.476 1.475	1.463 1.477	1.462	1.470	1.463	1.457 1.465*	1.467	1.479	1.453

Note: (a) Computational results obtained from DFT calculations at B3LYP/6 – 311 G(d,p) level of theory in gas phase; (b) obtained from crystal structure data in the Cambridge Structural Database with deposition numbers 684470, 214399, 1,124,824 respectively for compounds 2, 3, and 4. *Crystal structure data from our lab.

found between F4-O1 of the molecule, which is 0.250 Å less than the sum of their van der Waals radii. Similar intramolecular short contacts were observed between fluorine and oxygen in case of fluorinated benzoyl chloride compounds by Dey et al. [50] and halogen interactions by Resnati et al. [51] and Lu et al. [52]. Endoperoxide oxygen is involved in C-F-O non-covalent interaction and is not accessible to other atoms except fluorine due to steric effect (large perfluorooctyl chain). There are large numbers of intermolecular and intramolecular interactions in the crystal structure of compound 1. Intermolecular interactions include F···F, F···H, C···H, F···C interactions. Intramolecular interactions for compound 1 includes F···O, F···F, F···H, F···C interactions. There are no π - π interactions in the molecule due to the non-planarity of the structure, which is in line with the crystal structures of anthracene endoperoxide derivatives reported in the literature [10,53-55]. The distance between F20-O2 is 2.806 Å and F21-O2 is 2.803 Å, whereas the distance between F3-O1 is 2.976 Å and F4-O1 is 2.740 Å

Hirshfeld surface analysis is carried out to analyze the role of various interactions in the crystal structure. The spikes in 2D fingerprint plots of compound 1 (Fig. 3) indicate the close contacts over the Hirshfeld surface. Colors blue, yellow-red and length of spikes are indicative of strength of close contacts present in the crystal packing for compound 1. From the fingerprint plots, the dominant intermolecular interactions found to be F···F (55.9 %), F···H (26.2 %) contacts as the molecule contains plenty of F atoms. Besides the above intermolecular interactions, there are C···H (4.7 %), C···F(4.2 %) short contacts are present in the crystal packing of compound 1.

2.3. Computational insights

Table 1 summarizes the bond distances of anthracene endoperoxide derivatives in the solid state, measured from crystal structure data obtained from the Cambridge Structural Database (CSD), and compared with compound **1** in this work. The O-O bond length for compound **1** is 1.475 Å, which is shorter than that of 9,10-diphenyl-anthracene endoperoxide (compound 3) but is the same as 9,10-bismethyl-anthracene endoperoxide (compound 2). Smaller C-O bond distance was observed for compound 1 in comparison to data from the literature compounds 2, 3, 4 [53-55]. The O···O bond length of compound 1 is longer compared to the DFT calculation results of its CF3 substituted analog in the gas phase (Table 1). This indicates that the perfluorooctyl chain in compound 1 may provide additional electron withdrawing effect on oxygen through the fluorine on its β -carbon of the perfluorooctyl chain, as shown in Fig. 2 of the short F···O intramolecular interactions. Whereas the C-O bond length remains the same both in the crystal structure and the result from DFT calculations. Further comparing the O-O bond lengths from available crystal structures (compounds 2, 3, 4 in Table 1) and computed O-O bond lengths for the corresponding compounds, we find that phenyl group (compound 3) may also possess additional effect through space as methyl (compound 2) and non-substituted (compound 4) do not show significant difference between crystal structural data and DFT results. Together, these available experimental data and our computational results suggest that it warrants further in-depth investigation both experimentally and computationally of various anthracene endoperoxides in order to deeply understand how the 9,10-position substituents affect the degree of O—O bond activation, judged by its bond length change (Table 1).

To further understand how the perfluorooctyl substituents affect the endoperoxide stability, we performed a head-to-head comparison of compound 1 with n-octyl substituted anthracene endoperoxide by DFT calculation where the octyl chain maintained same conformation as the perfluorooctyl substituents. From Fig. 4, we observe that the strong electron withdrawing perfluorooctyl chains in compound 1, having similar electronic effect of CF $_3$ ($\sigma_p=0.54$), lowering both the HOMO, LUMO energies by around 0.8 eV in comparison to octyl ($\sigma_p=$ -0.17 for CH $_3$) chains of anthracene endoperoxide, stabilizing the anthracene endoperoxide from decomposition.

3. Conclusions

Perfluorooctyl anthracene endoperoxide is formed through photoirradiation of 9,10-bisperfluorooctyl- anthracene in solution in the presence of oxygen. ¹H NMR spectroscopy and single crystal XRD studies confirm the formation of compound 1 from the corresponding perfluoroalkylated anthracene. Intramolecular F···O short contacts are observed in the crystal structure of compound 1 that, at least partially, stabilize the anthracene endoperoxide from further decomposition. DFT

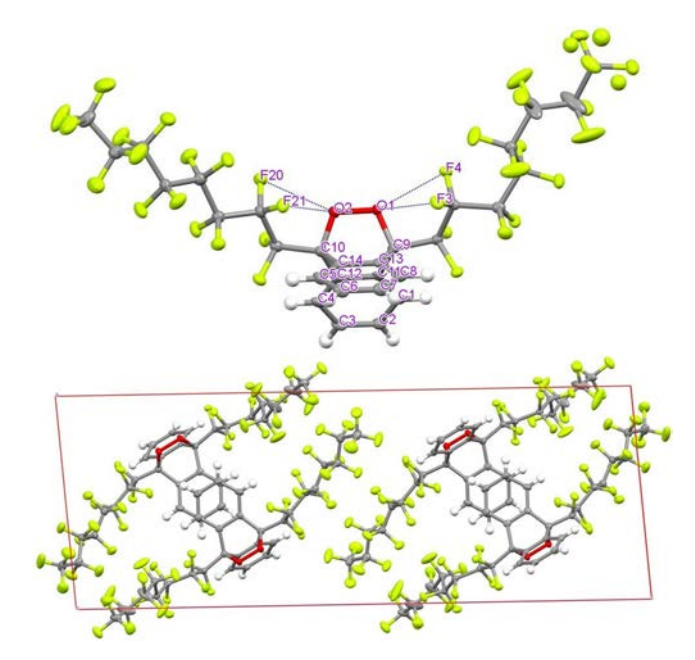


Fig. 2. Crystal structure, C—F···O short contacts and unit cell crystal packing of 9,10-bisperfluorooctyl-anthracene endoperoxide (compound 1). (gray: Carbon, light gray: Hydrogen, yellow: Fluorine, red: Oxygen). All other intramolecular contacts were omitted for clarity. Note: one of the terminal CF₃ groups on one perfluorooctyl chain has disorder due to rotation. This disorder was omitted in the unit cell packing for clarity. (For interpretation of the references to colour in this figure legend, the reader is referred to the web version of this article).

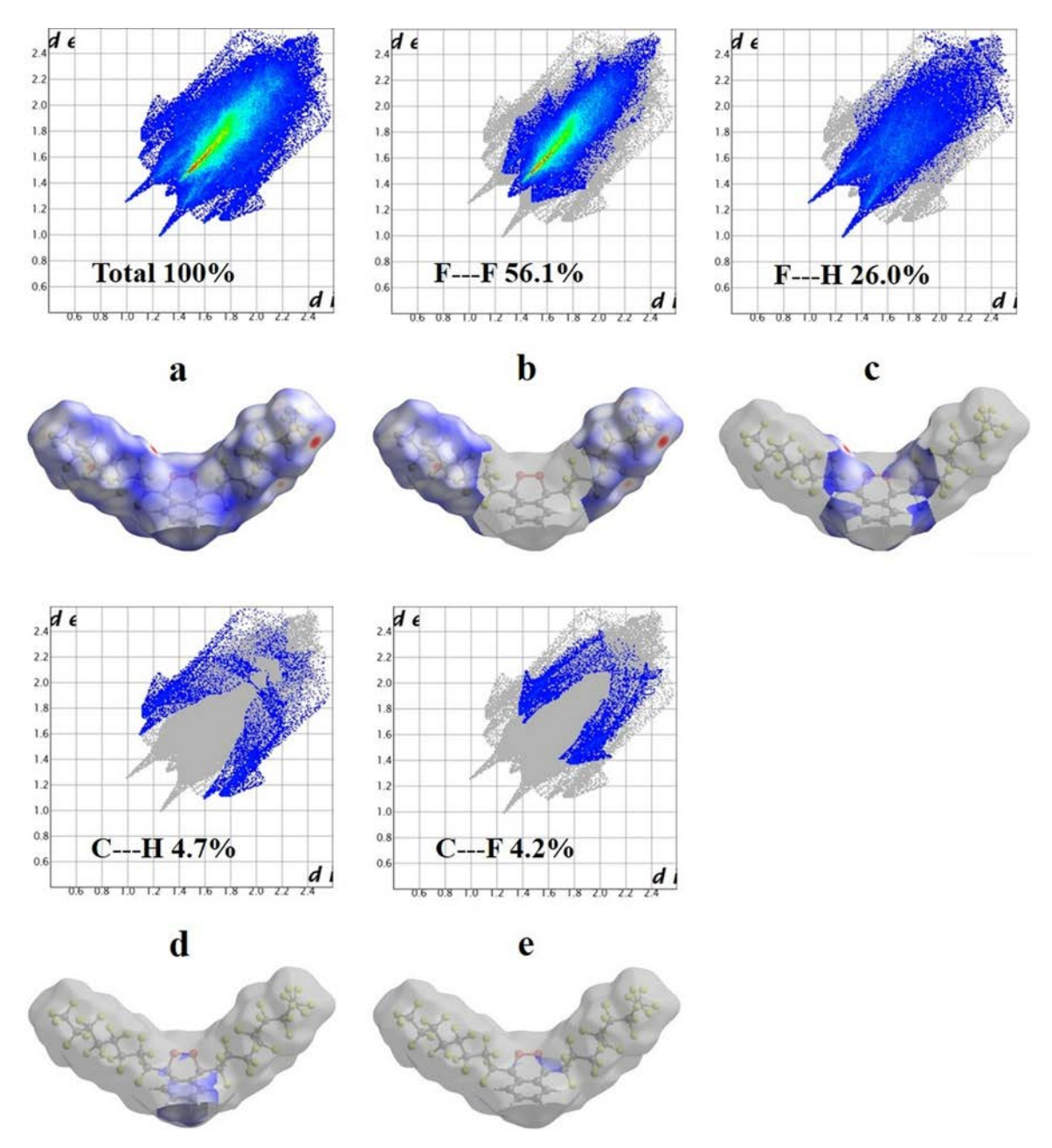


Fig. 3. 2D finger print plots and Hirshfeld surface view of the sum of intermolecular interactions (a), intermolecular interaction between F···F(b), F···H(c), C···H(d), C···F (e) in compound 1.

calculations show that both the HOMO and LUMO energies are lowered for compound 1 compared to the non-fluorinated analog that further supports the conclusion of perfluoroalkylation stabilizing anthracene endoperoxide. Computational results, together with available crystal structure data, of various anthracene endoperoxides imply that the O—O bond is not solely affected by the electronic effect of substituents through bonds, but may also be affected by the electronic effect through space, as shown in the crystal structure of compound 1. Further investigation both experimentally and computationally on how the substituents affect the endoperoxide bonding is needed.

4. Experimental section

All chemicals and solvents were purchased from commercial sources and used without further purification unless otherwise specified in the text. All NMR spectral studies were carried out using CDCl₃ unless otherwise specified. ¹H, ¹⁹F, and ¹³C NMR spectra were recorded on

JEOL 400 MHz, Bruker 400 MHz and Varian 200 MHz NMR spectrometers. NMR experiments for monitoring the formation of 9,10-bis-perfluorooctyl-anthracene endoperoxide (compound 1) were recorded using a Varian 200 MHz NMR spectrometer. NMR experiments for monitoring the formation of 9,10-bis(n-octyl)-anthracene endoperoxide were recorded using a Bruker 400 MHz NMR spectrometer. Mass spectra were recorded on a Varian 500-MS with ESI technique in positive ion detection mode. The infrared spectra were measured on a Bruker Alpha FTIR spectrometer with a diamond ATR crystal by directly placing solid sample on the ATR crystal surface with firm contact.

4.1. Synthesis

4.1.1. 9,10-Bisperfluorooctyl-anthracene endoperoxide (compound 1)

9,10-Bisperfluorooctyl-anthracene [56] (15 mg) was added into $CDCl_3$ in an NMR tube and exposed the solution to 300 W Xenon lamp at a distance of 30 cm with 1.5 AM filter for 20 min. Compound 1 was

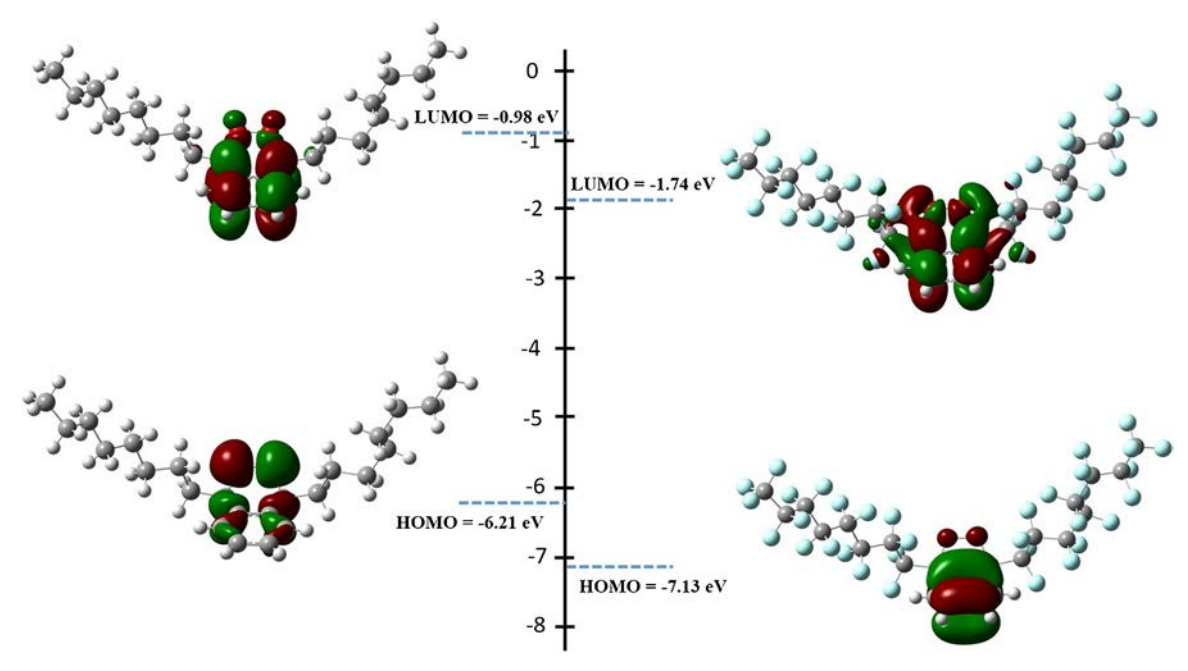


Fig. 4. HOMO-LUMO diagrams and corresponding energies. Left, 9,10-bis(n-octyl)- anthracene endoperoxide; Right, compound 1. Results were obtained from DFT calculations at B3LYP/6-311 G(d,p) level of theory in gas phase.

characterized by 1 H NMR (400 MHz, CDCl₃): δ 7.58 (br. S., 4 H), 7.34 (dd, J=5.5, 3.2 Hz, 4 H); 19 F NMR (376 MHz, CDCl₃): δ -80.58 (t, 20.2 Hz, 6 F), -114.49, -121.53, -122.57, -125.94; ESI-MS (positive ion mode)-Calcd. 1046.3, Found [M+H] $^+$: 1047.1; IR (solid sample on ATR, vibrational frequency in cm $^{-1}$): 529(s), 555(s), 635(m), 664(s), 708(m), 738(m), 762(m), 803(w), 918(w), 989(w), 1068(w), 1114(s), 1144(vs), 1196(vs), 1240(s), 1326(w), 1370(w), 1500(vw), aromatic C–H stretching was not clearly observed due to very week signals and poor sensitivity of the diamond ATR in the high frequency range.

4.1.2. 9,10-Bis(n-octyl)-anthracene: Synthesized from a modified procedure of Duerr et al [57]

9,10-Dibromo anthracene (2.0 g, 5.95 mmol) was added to a dry 100-mL round-bottomed flask, followed by 20 ml of anhydrous diethyl ether. The mixture was stirred for 10 min and added n-butyl lithium (6 ml of 2.6 M solution in hexane, 15.6 mmol) dropwise using syringe over a period of 40 min. The resulting mixture was stirred for 15 min and used this reaction mixture for next step without purification. Iodooctane (4.33 mL, 24 mmol) was added to the above reaction mixture and heated to reflux for 15 h. Then washed with water, dried over MgSO₄ and rotovapored to get yellow oil as a crude product. Crude product was subjected to column chromatography using hexane as eluent and evaporated the solvent to get yellow powder as product (782 mg, 32%). 9,10-bis(n-octyl)-anthracene was characterized by ¹H NMR (400 MHz, CDCl₃): δ 8.32 (q, J = 3.4 Hz, 4 H), 7.51 (q, J = 3.4 Hz, 4 H), 3.59 (t, J = 8.3 Hz, 4 H), 1.83 (p, J = 8.3 Hz, 4 H) 1.62 (p, J = 7.4 Hz, 4 H), 1.44 (m, 4 H), 1.32 (m, 12 H), 0.91 (t, J = 6.8 Hz, 6 H); 13 C NMR (100 MHz, CDCl₃): δ 133.9, 129.3, 125.2, 124.8, 31.9, 31.4, 30.4, 29.6, 29.4, 28.2, 22.7, 14.1; ESI-MS (positive ion mode)-Calcd. 402.6, Found [M+H]+: 403.4; IR (solid sample on ATR, vibrational frequency in cm⁻¹): 410, 597, 656, 724, 748, 787, 836, 946, 1005, 1028, 1122, 1179, 1377, 1379, 1456, 1462, 1485, 1528, 1617, 2847, 2917, 2947, 3076.

4.1.3. 9,10-Bis(n-octyl)-anthracene endoperoxide

Given its significant photochemical instability of 9,10-bis(n-octyl)-anthracene, which was demonstrated in our previous work [56], we carried out the photochemical synthesis of 9,10-bis(n-octyl)-anthracene endoperoxide under much weaker light intensity and stopped the

photochemical reaction after NMR spectra confirmed the product formation. 9,10-Bis(n-octyl)-anthracene (15 mg) was dissolved in CDCl₃ in NMR tube and exposed to 300 W Xenon lamp light, with a lamp to sample distance of 100 cm with an 1.5 AM filter, for 5 min of total reaction time. The reaction was periodically monitored by $^1\mathrm{H}$ NMR spectroscopy (Supporting information, Figure S11) to exam the endoperoxide formation progresses. This compound was characterized by $^1\mathrm{H}$ NMR (400 MHz, CDCl₃): δ 7.35 (q, 4 H), 7.24 (q, 4 H), 2.60 (t, 4 H), 1.84 (m, 4 H) 1.56 (m, 4 H), 1.45 (m, 4 H), 1.32 (m, 12 H), 0.91 (t, 6 H); and ESI-MS (positive ion mode)-Calcd.: 434.6, Found [M+H] $^+$: 435.4. Attempt of growing single crystal that is suitable for X-ray single crystal structure determination was not successful, perhaps due to its instability and flexible long alkyl chains that potentially hinder the crystal growth.

Single crystal X-ray diffraction data (CCDC deposition number 2003783) were collected using Mo K α radiation (λ = 0.71073 Å) on a Bruker CCD APEXII diffractometer at 100 K (Table 2). Crystal structure was solved using SHELXL-97 by direct method in conjunction with standard difference Fourier techniques and subsequently refined by full matrix least square analysis. All hydrogen atoms were placed in their ideal positions, and all non-hydrogen atoms except the occupancies (F15', F16', F17') were refined anisotropically. Using Mercury, intermolecular and intramolecular interactions with crystal packing were produced.

Hirshfeld surfaces and 2D fingerprint plots were generated using Crystal Explorer 17.5 from the experimental single crystal X-ray diffraction data. 2D fingerprint plots were generated for visualizing percentage contribution of each contact. A 2D fingerprint plot (di versus de) represents the presence of various intermolecular interactions in the crystal packing of a molecule.

All computational calculations were performed on Lawrence Supercomputer at the University of South Dakota. Gaussian-16 [58] and Gaussview-6.1 [59] interface programs were used for all the calculations, reading and interpreting results. Geometry optimization was done with DFT method at B3LYP/6 – 311 G(d,p) level of theory. All calculated geometries were checked with frequency calculation at B3LYP/6 – 311 G(d,p) level of theory to ensure each optimized geometry was a local minima. The bond distances (O—O and C—O) for various anthracene endoperoxides were measured from the optimized geometries.

Table 2Summary of crystal data, data collection, and structure refinement parameters for compound 1.

Crystal data					
Formula	C30 H8 F34 O2				
Formula weight	1046.3				
Temp, K	100				
Crystal setting	Monoclinic				
Space group	P21/c				
Hall symbol	-P 2ybc				
International tables number	14				
a, Å	12.477				
b, Å	8.117				
c, Å	33.539				
α, deg	90.00				
β, deg	94.598				
γ, deg	90.00				
z	4				
Cell volume (Å ³)	3386				
Density (diffrn), g cm ⁻³	2.053				
Absorb coefficient, mm ⁻¹	0.256				
F (000)	2040				
Data range $(\theta_{min} - \theta_{max})$	2.44 - 25.99				
Index ranges	\pm 15, \pm 10, \pm 4				
Measured reflections	32,733				
Independent reflections	6738				
Reflections with $I > 2\sigma(I)$	4348				
Max/Min trans	0.948/0.939				
Restraints/Parameters	0/610				
GOF	1.03				
$R [F^2 > 2\sigma(F^2)]$	0.071				
wR(F ²)	0.162				

Declaration of Competing Interest

There are no financial or intellectual conflicts of interest to declare.

Acknowledgements

Financial support from the NSF (CHE1355677) and the U.S. Army Research Office (grant number W911NF-09-10472) are greatly appreciated. Authors also acknowledge the South Dakota Governor's Office of Economic Development for providing financial support through the Center for Fluorinated Functional Materials. The authors thank NSF-MRI grants, CHE-1229035, for the purchase of a Bruker 400 MHz NMR spectrometer; and CHE-1919637, for the purchase of a Bruker Dual-Source Single-Crystal X-ray Diffractometer. Computations supporting this project were performed on the Lawrence High Performance Computing System at the University of South Dakota, funded by an NSF grant (ACI-1626516).

Appendix A. Supplementary data

Supplementary material related to this article can be found, in the online version, at doi:https://doi.org/10.1016/j.jfluchem.2020. 109548.

References

- W. Fudickar, T. Linker, Photoimaging with singlet oxygen at the solid air interface, Langmuir 25 (17) (2009) 9797–9803.
- [2] W. Fudickar, T. Linker, Novel anthracene materials for applications in lithography and reversible photoswitching by light and air, Langmuir 26 (6) (2010) 4421–4428.
- [3] Z. Gao, Y. Han, F. Wang, Cooperative supramolecular polymers with anthracene-endoperoxide photo-switching for fluorescent anti-counterfeiting, Nat. Commun. 9 (1) (2018) 3977.
- [4] F. Grellepois, F. Chorki, M. Ourévitch, S. Charneau, P. Grellier, K.A. McIntosh, W.N. Charman, B. Pradines, B. Crousse, D. Bonnet-Delpon, J.-P. Bégué, Orally active antimalarials: hydrolytically stable derivatives of 10-Trifluoromethyl anhydrodihydroartemisinin, J. Med. Chem. 47 (6) (2004) 1423–1433.

- [5] Y. Jing, Q. Xu, M. Chen, X. Shao, Pyridone-containing phenalenone-based photosensitizer working both under light and in the dark for photodynamic therapy, Biorg. Med. Chem. 27 (11) (2019) 2201–2208.
- [6] S. Callaghan, M.O. Senge, The good, the bad, and the ugly controlling singlet oxygen through design of photosensitizers and delivery systems for photodynamic therapy, Photochem. Photobiol. Sci. 17 (11) (2018) 1490–1514.
- [7] M.A. Filatov, M.O. Senge, Molecular devices based on reversible singlet oxygen binding in optical and photomedical applications, Mol. Syst. Des. Eng. 1 (3) (2016) 258–272.
- [8] C. Schweitzer, R. Schmidt, Physical mechanisms of generation and deactivation of singlet oxygen, Chem. Rev. 103 (5) (2003) 1685–1758.
- [9] M.C. DeRosa, R.J. Crutchley, Photosensitized singlet oxygen and its applications, Coord. Chem. Rev. 233-234 (2002) 351–371.
- [10] J.-M. Aubry, C. Pierlot, J. Rigaudy, R. Schmidt, Reversible binding of oxygen to aromatic compounds, Acc. Chem. Res. 36 (9) (2003) 668–675.
- [11] Y. Yuan, C.-J. Zhang, S. Xu, B. Liu, A self-reporting AIE probe with a built-in singlet oxygen sensor for targeted photodynamic ablation of cancer cells, Chem. Sci. 7 (3) (2016) 1862–1866.
- [12] J. Park, D. Feng, S. Yuan, H.-C. Zhou, Photochromic metal-organic frameworks: reversible control of singlet oxygen generation, Angew. Chem. Int. Ed. 54 (2) (2015) 430–435.
- [13] J. Ge, M. Lan, B. Zhou, W. Liu, L. Guo, H. Wang, Q. Jia, G. Niu, X. Huang, H. Zhou, X. Meng, P. Wang, C.-S. Lee, W. Zhang, X. Han, A graphene quantum dot photo-dynamic therapy agent with high singlet oxygen generation, Nat. Commun. 5 (2014) 4596.
- [14] S. Kolemen, T. Ozdemir, D. Lee, G.M. Kim, T. Karatas, J. Yoon, E.U. Akkaya, Remote-controlled release of singlet oxygen by the plasmonic heating of endoperoxide-modified gold nanorods: towards a paradigm change in photodynamic therapy, Angew. Chem. Int. Ed. 55 (11) (2016) 3606–3610.
- [15] W. Fudickar, T. Linker, Release of singlet oxygen from aromatic endoperoxides by chemical triggers, Angew. Chem. Int. Ed. 57 (39) (2018) 12971–12975.
- [16] V.R. Hathwar, M.K. Thomsen, M.A.H. Mamakhel, M.Ø. Filsø, J. Overgaard, B.B. Iversen, Electron density analysis of the "O-O" charge-shift bonding in rubrene endoperoxide, J. Phys. Chem. A 120 (38) (2016) 7510-7518.
- [17] J.T. Ly, S.A. Lopez, J.B. Lin, J.J. Kim, H. Lee, E.K. Burnett, L. Zhang, A. Aspuru-Guzik, K.N. Houk, A.L. Briseno, Oxidation of rubrene, and implications for device stability, J. Mater. Chem. C Mater. Opt. Electron. Devices 6 (14) (2018) 3757–3761.
- [18] C. Pierlot, J. Poprawski, J. Marko, J.-M. Aubry, Effects of oxygenated substituents on the [4+2] cycloaddition of singlet oxygen in the photooxygenation of watersoluble naphthyl ethers, Tetrahedron Lett. 41 (26) (2000) 5063–5067.
- [19] G.R. Martinez, J.-L. Ravanat, M.H.G. Medeiros, J. Cadet, P. Di Mascio, Synthesis of a naphthalene endoperoxide as a source of 18O-labeled singlet oxygen for mechanistic studies, J. Am. Chem. Soc. 122 (41) (2000) 10212–10213.
- [20] S. Martins, J.P.S. Farinha, C. Baleizão, M.N. Berberan-Santos, Controlled release of singlet oxygen using diphenylanthracene functionalized polymer nanoparticles, Chem. Commun. (Camb.) 50 (25) (2014) 3317–3320.
- [21] J. Zhu, J. Zou, J. Zhang, Y. Sun, X. Dong, Q. Zhang, An anthracene functionalized BODIPY derivative with singlet oxygen storage ability for photothermal and continuous photodynamic synergistic therapy, J. Mater. Chem. B Mater. Biol. Med. 7 (20) (2019) 3303–3309.
- [22] H.H. Wasserman, J.R. Scheffer, Singlet oxygen reactions from photoperoxides, J. Am. Chem. Soc. 89 (12) (1967) 3073–3075.
- [23] H. Fidder, A. Lauer, W. Freyer, B. Koeppe, K. Heyne, Photochemistry of Anthracene-9,10-endoperoxide, J. Phys. Chem. A 113 (22) (2009) 6289–6296.
- [24] H. Kotani, K. Ohkubo, S. Fukuzumi, Photocatalytic oxygenation of Anthracenes and olefins with Dioxygen via selective radical coupling using 9-Mesityl-10-methylacridinium ion as an effective electron-transfer photocatalyst, J. Am. Chem. Soc. 126 (49) (2004) 15999–16006.
- [25] I. Corral, L. González, A. Lauer, W. Freyer, H. Fidder, K. Heyne, Identifying the low-lying electronic states of anthracene-9,10-endoperoxide, Chem. Phys. Lett. 452 (1) (2008) 67–71.
- [26] W. Drews, R. Shimidt, H.D. Brauer, The photolysis of the endoperoxide of 9,10-Diphenylanthracene, Chem. Phys. Lett. 70 (1) (1980) 84–88.
- [27] M. Bauch, M. Klaper, T. Linker, Intermediates in the cleavage of endoperoxides, J. Phys. Org. Chem. 30 (4) (2017) e3607.
- [28] P. Vierling, C. Santaella, J. Greiner, Highly fluorinated amphiphiles as drug and gene carrier and delivery systems, J. Fluorine Chem. 107 (2) (2001) 337–354.
- [29] K. Haranahalli, T. Honda, I. Ojima, Recent progress in the strategic incorporation of fluorine into medicinally active compounds, J. Fluorine Chem. 217 (2019) 29–40.
- [30] K.L. Kirk, Fluorine in medicinal chemistry: recent therapeutic applications of fluorinated small molecules, J. Fluorine Chem. 127 (8) (2006) 1013–1029.
- [31] C.E. O'Hanlon, K.G. Amede, M.R. O'Hear, J.M. Janjic, NIR-labeled perfluoropolyether nanoemulsions for drug delivery and imaging, J. Fluorine Chem. 137 (2012) 27–33.
- [32] T. Fujiwara, D. O'Hagan, Successful fluorine-containing herbicide agrochemicals, J. Fluorine Chem. 167 (2014) 16–29.
- [33] T. Mori, K. Ujihara, O. Matsumoto, K. Yanagi, N. Matsuo, Synthetic studies of fluorine-containing compounds for household insecticides, J. Fluorine Chem. 128 (10) (2007) 1174–1181.
- [34] A. Tressaud, H. Groult, Fluorinated carbonaceous nanoparticles as active material in primary lithium battery, J. Fluorine Chem. 219 (2019) 1–9.
- [35] J. Lucas, F. Smektala, J.L. Adam, Fluorine in optics, J. Fluorine Chem. 114 (2) (2002) 113–118.
- [36] P. Kirsch, Fluorine in liquid crystal design for display applications, J. Fluorine Chem. 177 (2015) 29–36.
- [37] T. Nakajima. Fluorine compounds as energy conversion materials. J. Fluorine

- Chem. 149 (2013) 104-111.
- [38] K.C. Lowe, Fluorinated blood substitutes and oxygen carriers, J. Fluorine Chem. 109 (1) (2001) 59–65.
- [39] V.P. Reddy, Chapter 5 organofluorine pharmaceuticals, in: V.P. Reddy (Ed.), Organofluorine Compounds in Biology and Medicine, Elsevier, Amsterdam, 2015, pp. 133–178.
- [40] H. Sun, A. Putta, M. Billion, Arene Trifluoromethylation: An Effective Strategy to Obtain Air-Stable n-Type Organic Semiconductors with Tunable Optoelectronic and Electron Transfer Properties, J. Phys. Chem. A 116 (30) (2012) 8015–8022.
- [41] L.K. San, S.N. Spisak, C. Dubceac, S.H.M. Deng, I.V. Kuvychko, M.A. Petrukhina, X.-B. Wang, A.A. Popov, S.H. Strauss, O.V. Boltalina, Experimental and DFT studies of the electron-withdrawing ability of perfluoroalkyl (RF) groups: electron affinities of PAH(RF)n increase significantly with increasing RF chain length, Chem. Eur. J. 24 (6) (2018) 1441–1447.
- [42] I.V. Kuvychko, K.P. Castro, S.H.M. Deng, X.-B. Wang, S.H. Strauss, O.V. Boltalina, Taming hot CF3 radicals: incrementally tuned families of polyarene Electron acceptors for air-stable molecular optoelectronics, Angew. Chem. Int. Ed. 52 (18) (2013) 4871–4874.
- [43] R. Schmidt, M.M. Ling, J.H. Oh, M. Winkler, M. Könemann, Z. Bao, F. Würthner, Core-fluorinated perylene bisimide dyes: air stable n-Channel organic semiconductors for thin film transistors with exceptionally high on-to-Off current ratios, Adv. Mater. 19 (21) (2007) 3692–3695.
- [44] B.A. Jones, A. Facchetti, M.R. Wasielewski, T.J. Marks, Tuning Orbital Energetics in Arylene Diimide Semiconductors. Materials Design for Ambient Stability of n-Type Charge Transport, J. Am. Chem. Soc. 129 (49) (2007) 15259–15278.
- [45] H. Omorodion, B. Twamley, J.A. Platts, R.J. Baker, Further evidence on the importance of fluorous–fluorous interactions in supramolecular chemistry: a combined structural and computational study, Cryst. Growth Des. 15 (6) (2015) 2835–2841.
- [46] H. Sun, U.K. Tottempudi, J.D. Mottishaw, P.N. Basa, A. Putta, A.G. Sykes, Strengthening π-π interactions while suppressing Csp2-H··π (T-Shaped) interactions via perfluoroalkylation: a crystallographic and computational study that supports the beneficial formation of 1-D π-π stacked aromatic materials, Cryst. Growth Des. 12 (11) (2012) 5655–5662.
- [47] A. Putta, J.D. Mottishaw, Z. Wang, H. Sun, Rational design of lamellar π-π stacked organic crystalline materials with short interplanar distance, Cryst. Growth Des. 14 (1) (2014) 350–356.

- [48] A. Facchetti, M.-H. Yoon, C.L. Stern, G.R. Hutchison, M.A. Ratner, T.J. Marks, Building Blocks for N-Type Molecular and Polymeric Electronics. Perfluoroalkylversus Alkyl-Functionalized Oligothiophenes (nTs; n = 2-6). Systematic Synthesis, Spectroscopy, Electrochemistry, and Solid-State Organization, J. Am. Chem. Soc. 126 (41) (2004) 13480–13501.
- [49] M.A. Spackman, D. Jayatilaka, Hirshfeld surface analysis, CrystEngComm 11 (1) (2009) 19–32.
- [50] D. Dey, S. Bhandary, A. Sirohiwal, V.R. Hathwar, D. Chopra, "Conformational lock" via unusual intramolecular C-F···O=C and C-H···Cl-C parallel dipoles observed in in situ cryocrystallized liquids, Chem. Commun. (Camb.) 52 (45) (2016) 7225–7228
- [51] V. Kumar, D.J. Mulder, G. Cavallo, T. Pilati, G. Terraneo, G. Resnati, A.P.H.J. Schenning, P. Metrangolo, Structural characterization of new fluorinated mesogens obtained through halogen-bond driven self-assembly, J. Fluorine Chem. 198 (2017) 54-60.
- [52] V. Elakkat, C.-C. Chang, J.-Y. Chen, Y.-C. Fang, C.-R. Shen, L.-K. Liu, N. Lu, The first two examples of halogen bonding with a sigma hole-donating fluorine in the Csp3-F-Osp3 interaction from polyfluorinated trans-dihalo-palladium(II) di-substituted pyridine complexes, Chem. Commun. (Camb.) 55 (95) (2019) 14259–14262.
- [53] A. Usman, H.-K. Fun, Y. Li, J.-H. Xu, 9,10-Diphenyl-9,10-epidioxyanthracene and 9,10-dihydro-10,10-dimethoxy-9-phenylanthracen-9-ol, Acta Cryst. C 59 (6) (2003) 0308–0310.
- [54] Y.-W. Wang, 9,10-Dimethyl-9,10-peroxy-9,10-dihydroanthracene, Acta Cryst. E 64 (4) (2008) 0660.
- [55] C.J. Brown, M. Ehrenberg, 9,10-Dihydro-9,10-epidioxyanthracene, C14H10O2, Acta Cryst. C 40 (6) (1984) 1059–1060.
- [56] H. Sun, A. Putta, J.P. Kloster, U.K. Tottempudi, Unexpected photostability improvement of aromatics in polyfluorinated solvents, Chem. Commun. (Camb.) 48 (99) (2012) 12085–12087.
- [57] B.F. Duerr, Y.S. Chung, A.W. Czarnik, Syntheses of 9,10-disubstituted anthracenes derived from 9,10-dilithioanthracene, J. Org. Chem. 53 (9) (1988) 2120–2122.
- [58] M.J. Frisch, G.W. Trucks, H.B. Schlegel, G.E. Scuseria, M.A. Robb, J.R. Cheeseman, et al., Gaussian 16 Rev. C.01, Wallingford, CT, (2016).
- [59] Roy Dennington, Todd A. Keith, John M. Millam, GaussView, Semichem Inc., Shawnee Mission, KS, 2016.